[46]R. Ingalls, Phys. Rev. 188, 1045 (1969).
[47]C. E. Johnson, W. Marshall, and G. J. Perlow, Phys. Rev. 126, 1503 (1962), and references contained therein.
[48]G. W. Robinson, J. Mol. Spectry. 6, 58 (1961).

PHYSICAL REVIEW B VOLUME 4, NUMBER 11 1 DECEMBER 1971

Effect of Exchange with Local Moments and Hyperfine Interaction on the Electron-Spin-Resonance Line Shape in Metals*

J. H. Pifer and R. T. Longo†
Physics Department, Rutgers University, New Brunswick, New Jersey 08903
(Received 10 February 1971; revised manuscript received 25 June 1971)

The electron-spin-resonance and transmission-resonance line shapes in a metal containing impurities with local moments are evaluated for arbitrary exchange, hyperfine interaction, and nuclear spin using the Bloch-like equations derived by Langreth, Cowan, and Wilkins. Classical skin-depth conditions are assumed and the drift current produced by the gradient in the magnetic field is included in the diffusion term. Computer evaluation and a physical interpretation of the results are given. The theory is compared with the experimental transmission-resonance data in Cu : Mn. It is shown that the anomalies in the data are due to hyperfine interaction and a breakdown of strong coupling at low temperatures.

I. INTRODUCTION

When Owen, Browne, Knight, and Kittel[1] first examined the electron-spin-resonance (ESR) of a magnetic impurity in a metal (Mn in Cu) they expected to observe a large g shift and line broadening of the impurity resonance due to exchange interaction with the conduction electrons. Instead, they found a narrow line near $g = 2$. Hasegawa[2] explained the data in terms of a two-part system composed of the magnetic impurity magnetization $\vec{M}_d$ and the conduction-electron magnetization $\vec{M}_s$ which relaxes to the lattice with spin-lattice relaxation time T_{sl} and cross relaxes to $\vec{M}_d$ with a time T_{sd}. By detailed balance T_{ds}, the d to s cross relaxation time is related to T_{sd} by the relation $T_{ds} = \chi_r^0 T_{sd}$, where χ_r^0 is the ratio of the impurity susceptibility χ_d^0 to the conduction-electron susceptibility χ_s^0. Hasegawa pointed out that when $\vec{M}_d$ relaxes to $\vec{M}_s$ the energy does not necessarily flow to the lattice but may be returned to $\vec{M}_d$ via T_{sd}. This double cross relaxation has the same effect as no relaxation at all. Thus, $T_{1\,eff}$, the effective relaxation time of $\vec{M}_d$, depends on the size of T_{sl} relative to T_{sd}. Hasegawa showed that

$$T_{1\,eff} = T_{ds}(T_{sd} + T_{sl})/T_{sd} .$$

When $T_{sl} \ll T_{sd}$, $T_{1\,eff} = T_{ds} = \chi_r^0 T_{sd}$; but when $T_{sl} \gg T_{sd}$, $T_{1\,eff} = T_{sl}\chi_r^0$. In this latter case, where $T_{1\,eff}$ is controlled by T_{sl}, the relaxation is commonly said to be bottlenecked.[3] Hasegawa also explained the lack of g shift by pointing out that when $\vec{M}_s$ and $\vec{M}_d$ have fully cross relaxed (i.e., $\vec{M}_d$ is bottlenecked) they will be parallel and unable to exert a torque on each other.

Schultz and co-workers[4,5] have used Hasegawa's model to explain the transmission-electron-spin-resonance (TESR) data for various transition impurities in copper and silver. They assumed bottleneck conditions and explained that the observed temperature-dependent g shift was due to the inequality of g_s, the conduction-electron g value, and g_d, the impurity g value. In TESR, dilute alloys are used so that at high temperature $\chi_s^0 \gg \chi_d^0$ and the g value is near g_s. At low temperature, where $\chi_d^0 \gg \chi_s^0$, the magnetic impurity dominates the resonance signal and the g value moves down to g_d. In order to explain the linewidth data it was necessary to add an impurity spin-lattice relaxation time T_{dl}, which was comparable in size to T_{sl}.

From the TESR viewpoint, the term bottleneck is a rather unfortunate choice of terminology since it is more logical to consider the conduction electrons on the same basis as the magnetic impurities rather than as a reservoir through which $\vec{M}_d$ relaxes. In addition, one normally expects that when a bottleneck is broken the relaxation will be faster, but as the term is now used, $T_{1\,eff}$ becomes much slower (if T_{sl} is kept constant) as the bottleneck is broken.

Hasegawa described the exchange-coupled system with two Bloch-like equations coupled to each other by the cross relaxation and by molecular or exchange fields. These phenomenological equations have been put on a better footing by Langreth, Cowan, and Wilkins[6] (LCW) who showed from first principles that coupled Bloch-like equations properly describe the system in the limit $\gamma\hbar H_0 \ll kT$, where

H_0 is the applied magnetic field and T is the temperature. They included the hyperfine interaction with the impurity nucleus which had previously been ignored, and showed that contrary to Hasegawa's assumption, the spin lattice and cross relaxation proceed toward the instantaneous equilibrium magnetization. The hyperfine interaction enters into the problem extremely simply, appearing only in the local magnetic field that each magnetic impurity experiences. One might expect that it should appear in the molecular field that the conduction electrons experience. However, as an electron moves through the sample it encounters many magnetic impurities during its spin lifetime. For dilute samples no interaction occurs between impurities so all nuclear orientations are equally probable and the hyperfine interaction averages to zero. Likewise, all spatial dependence of the exchange interaction is averaged away and only the long-wavelength component remains.

In order to get the ESR or TESR line shape it is necessary to treat the diffusion of the conduction electrons. Kaplan[7] has treated diffusion in the conduction-electron spin resonance (CESR) of pure samples by adding a diffusion term proportional to $\nabla^2\vec{M}_s$ to the Bloch equation in a manner analogous to Torrey's[8] treatment of the resonance of diffusing nuclei in a liquid. This method gives excellent agreement with experiments[9,10] and has been shown[11] to be equivalent to Dyson's[12] Green's-function approach. Walker[13] has pointed out that the drift current produced by the gradient in the magnetic field (which was included in Torrey's treatment but not carried by Kaplan) can be much larger than the diffusion current in the skin region. This added term cancels for CESR in a pure sample, but must be carried for any more complicated calculation. Kaplan's treatment of the diffusion is valid only for classical skin conditions. Lampe and Platzman[14] have shown that the signal can be written as the product of resonant-spin terms times a power of the surface impedance for spinless electrons. In order to treat the anomalous skin conditions one must then only evaluate the anomalous surface impedance. This procedure, using Reuter and Sondheimer's[15] calculation of the anomalous surface impedance, gives excellent agreement with experiments[10] in pure samples. Walker has questioned this approach, pointing out that the assumption that the diffusion is driven by $\nabla\vec{M}_s$ limits one to classical skin conditions.

In this paper we solve the LCW equations for both the ESR and TESR line shapes with any strength exchange including hyperfine interaction with arbitrary nuclear spin. We include T_{d1} relaxation and the drift current term, but we do not treat the anomalous skin effect. Anomalous skin conditions should not occur in very concentrated alloys due to the short mean free path. However, our chief reason for not including it, apart from the question of whether Lampe and Platzman's approach is valid at all, is that it adds considerable complexity and an additional parameter without adding anything that will change the basic physical interpretation. The interaction responsible for the rapid T_{d1} relaxation is not understood since the effect of relaxation by the conduction electrons is treated as cross relaxation. However, we include the T_{d1} term since it appears to be physically necessary.

We will discuss our results using a combination of analytical expansion in various limits and computer evaluation in order to present a physical interpretation of the manner in which the transition is made from weak to strong coupling and of the effects of hyperfine interaction. In our discussion we will avoid talking in terms of the bottleneck. We find that T_{ds} is the natural time to use and that the character of the resonance depends on the size of T_{ds}, relative not only to T_{s1} but also to T_{d1}, the separation of the two resonances, and the hyperfine splitting.

II. CALCULATION OF LINE SHAPE

We assume that a steady magnetic field $H_0\hat{z}$ is applied perpendicular to the flat sample and that the transverse components of the electric field $\vec{E}$, magnetic field $\vec{H}$, and a total magnetization $\vec{M}$, vary as $e^{i\omega t \pm kz}$. The displacement current can be neglected inside the metal so that Maxwell's equations become

$$\nabla\times\vec{E}=\frac{1}{c}\left(\frac{\partial\vec{H}}{\partial t}+4\pi\frac{\partial\vec{M}}{\partial t}\right), \tag{1}$$

$$\nabla\times\vec{H}=(4\pi\sigma/c)\vec{E}\,. \tag{2}$$

In order to obtain the ESR and TESR line shapes, we must solve these equations for the rf fields inside the sample. The calculation is complicated because the relation between $\vec{M}$ and rf magnetic field is nonlocal due to the diffusion of the electrons. Dyson[12] solved for $\vec{M}$ in a pure sample by expressing it as an integral of a Green's function over the diffusion and relaxation probabilities. Kaplan[7] pointed out that the problem could be solved much more simply by assuming that $\vec{M}$ is described by a Bloch equation, as modified for diffusion by Torrey.[8] When magnetic impurities with no hyperfine interaction are added, two Bloch equations are needed, one for the conduction-electron (s-spin) magnetization $\vec{M}_s$, and one for the magnetic (d-spin) magnetization $\vec{M}_d$. However, when we consider the nuclear hyperfine interaction, the problem is more complicated since the torque that an electron experiences depends on the effective magnetic field that it sees. A nucleus of spin I has $2I+1$ orientations so that we need a separate equation to describe the d magnetization $\vec{M}_{dm}$ in each of the

$2I+1$ possible environments in which a d spin might find itself. This problem has been considered theoretically by LCW who derived the following appropriate Bloch-like equations:

$$\frac{d\vec{M}_s}{dt} = \gamma_s \vec{M}_s \times (\vec{H} + \alpha \vec{M}_d) - \frac{1}{T_{sl}} [\vec{M}_s - \chi_s^0 (\vec{H} + \alpha \vec{M}_d)] - \frac{1}{T_{sd}} [\vec{M}_s - \chi_s^0 (\vec{H} + \alpha \vec{M}_d)] + \frac{1}{T_{ds}} [\vec{M}_d - \chi_d^0 (\vec{H} + \alpha \vec{M}_s)] + D\nabla^2 [\vec{M}_s - \chi_s^0 (\vec{H} + \alpha \vec{M}_d)] , \quad (3)$$

$$\frac{d\vec{M}_m}{dt} = \gamma_d \vec{M}_m \times (\vec{H} + \vec{H}_m + \alpha \vec{M}_s) - \frac{1}{T_{dl}} \left(\vec{M}_m - \frac{\chi_d^0}{2I+1} (\vec{H} + \alpha \vec{M}_s) \right) - \frac{1}{T_{ds}} \left(\vec{M}_m - \frac{\chi_d^0}{2I+1} (\vec{H} + \alpha \vec{M}_s) \right) + \frac{1}{2I+1} \frac{1}{T_{sd}} [\vec{M}_s - \chi_s^0 (\vec{H} + \alpha \vec{M}_d)] , \quad (4)$$

where $m = -I, \ldots, I-1, I$. α is the exchange field constant and to lowest order in J is equal to $\frac{1}{2}J\rho$, where J is the exchange integral and ρ is the density of states per electron at the Fermi surface. H_m is the hyperfine field

$$\vec{H}_m = m A_{hf} \hat{z} \quad (5)$$

and

$$\vec{M}_d = \sum_{m=-I}^{I} \vec{M}_{dm} . \quad (6)$$

We shall assume for all numerical calculations that T_{ds} is given by the first-order perturbation expression given by LCW:

$$\frac{1}{T_{ds}} = \frac{4\pi k}{\hbar} (\alpha \chi_s^0)^2 \frac{\chi_r^0(1)}{\chi_r^0} , \quad (7)$$

where $\chi_r^0 \equiv \chi_r^0(1)/T$ is assumed to have a Curie behavior. T_{sd} is related by T_{ds} by $T_{ds} = \chi_r^0 T_{sd}$. We have slightly generalized the LCW equations by letting γ_s differ from γ_d and by adding the T_{dl} term. These equations differ somewhat from the phenomenological equations previously used for $I=0$ in that relaxation is toward the instantaneous equilibrium magnetization. These differences are important since the equations now give the correct static susceptibilities

$$\chi_s = \chi_s^0 (1 + \alpha \chi_d^0) / (1 - \alpha^2 \chi_s^0 \chi_d^0) , \quad (8)$$

$$\chi_d = \chi_d^0 (1 + \alpha \chi_s^0) / (1 - \alpha^2 \chi_s^0 \chi_d^0) . \quad (9)$$

The difference between χ_d and χ_d^0 is slight since the Pauli susceptibility χ_s^0 is small and temperature independent. But note that, since χ_d^0 obeys a Curie law, χ_s passes through zero and reverses sign for negative exchange as the temperature is decreased. This simply corresponds to the exchange field becoming stronger than the applied field. Thus, χ_s can depend strongly on temperature even though χ_s^0 does not.

Another difference between Eq. (3) and previous treatments is in the diffusion term, where we have included a drift current term. Without this drift correction Eq. (3) does not have the proper steady-state solution $M_s = \chi_s^0 (H + \alpha M_d)$.

Note that although Eqs. (3) and (4) appear to be very complicated, they are, in fact, very simple, stating, for example, that the time change of $\vec{M}_s$ at some point in the sample is due to the torque of the resultant effective magnetic field plus the spin-lattice relaxation toward the instantaneous equilibrium magnetization, the cross relaxation, and the electron diffusion.

Equations (1) and (2) can be rewritten, using complex notation and dimensionless variables, as

$$-4\pi i \epsilon^2 \mathfrak{M} + (K^2 - i\epsilon^2) \mathcal{H} = 0 , \quad (10)$$

$$\mathcal{E} = \frac{-ic}{4\pi\sigma} \frac{\partial \mathcal{H}}{\partial z} , \quad (11)$$

where

$$\mathfrak{M} = \mathfrak{M}_d + \mathfrak{M}_s , \quad \mathfrak{M}_s = M_{sx} - i M_{sy} , \quad \mathfrak{M}_d = M_{dx} - i M_{dy} ,$$

$$\mathcal{E} = E_x - i E_y , \quad \mathcal{H} = H_x - i H_y , \quad K^2 = \tfrac{1}{2} k^2 \delta_e^2 ,$$

$$\epsilon = \delta_e / \delta , \quad \delta_e = (2DT_{sl})^{1/2} , \quad \delta = (c^2 / 2\pi\sigma\omega)^{1/2} .$$

δ is the skin depth, δ_e is the spin depth, i.e., the distance a spin can diffuse before relaxing, and K is the dimensionless propagation constant.

The $2I+2$ equations given by Eqs. (3) and (4) can be written in the form

$$(A - K^2) \mathfrak{M}_s + (B + \alpha \chi_s^0 K^2) \mathfrak{M}_d + \chi_s^0 (C + K^2) \mathcal{H} = 0 , \quad (12)$$

$$E \mathfrak{M}_s + G_m \mathfrak{M}_{dm} + J \mathfrak{M}_d + \chi_s^0 F \mathcal{H} = 0 , \quad (13)$$

where

$$A = 1 + (1 + \alpha \chi_s^0) T_{sl} / T_{sd} + i T_{sl} [\omega - \omega_s (1 + \alpha \chi_d)] , \quad (14)$$

$$B = -T_{sl} (1 + \alpha \chi_s^0 \chi_r^0) / (T_{sd} \chi_r^0) - \alpha \chi_s^0 + i \alpha \chi_s \omega_s T_{sl} , \quad (15)$$

$$C = -1 + i\omega_s T_{s1}\chi_s/\chi_s^0 , \tag{16}$$

$$E = \frac{-\alpha\chi_d^0}{T_{d1}} - \frac{1+\alpha\chi_s^0}{T_{sd}} + i\alpha\chi_d\omega_d\frac{T_{s1}}{2I+1} , \tag{17}$$

$$G_m = \left(\frac{1}{T_{d1}} + \frac{1}{T_{sd}\chi_r^0} + i[\omega - \omega_d(1+\alpha\chi_s) - m\omega_{hf}]\right)T_{s1} , \tag{18}$$

$$J = \alpha\chi_s^0 T_{s1}/[T_{sd}(2I+1)] , \tag{19}$$

$$F = \left(\frac{-\chi_r^0}{T_{d1}} + \frac{i\omega_d\chi_d}{\chi_s^0}\right)\frac{T_{s1}}{2I+1} , \tag{20}$$

with

$$\chi_r = \chi_d/\chi_s , \quad \chi_r^0 = \chi_d^0/\chi_s^0 , \quad \omega_{hf} = \gamma_d A_{hf} ,$$

$$\omega_s = \gamma_s H_0 , \quad \omega_d = \gamma_d H_0 , \quad \mathfrak{M}_d = \sum_{m=-I}^{I}\mathfrak{M}_{dm} .$$

To have a nontrivial solution, the determinant of the coefficients of Eqs. (12), (13), and (10) must be zero:

$$\begin{vmatrix} A - i\epsilon^2 - X^2 & B' + \alpha\chi_s^0 X^2 & B' + \alpha\chi_s^0 X^2 & \cdots & B' + \alpha\chi_s^0 X^2 & \chi_s^0(C + i\epsilon^2 + X^2) \\ E & G(-I)+J & J & \cdots & J & \chi_s^0 F \\ E & J & G(-I+1)+J & \cdots & J & \chi_s^0 F \\ \cdots & \cdots & \cdots & \cdots & \cdots & \cdots \\ E & J & J & \cdots & G(I)+J & \chi_s^0 F \\ -4\pi i\epsilon^2 & -4\pi i\epsilon^2 & -4\pi i\epsilon^2 & \cdots & -4\pi i\epsilon^2 & X^2 \end{vmatrix} = 0 , \tag{21}$$

where $B' = B + \alpha\chi_s^0 i\epsilon^2$ and $X^2 = K^2 - i\epsilon^2$. Because of the high symmetry this is easily solved to give the following quadratic equation in X^2:

$$X^4 - C_1 X^2 + C_2 = 0 , \tag{22}$$

where

$$C_1 = C_{10} + \chi_s^0 C_{11} , \quad C_2 = C_{21}\chi_s^0 ,$$

and

$$C_{10} = [A - i\epsilon^2 - B'E/(U+J)]V , \tag{23}$$

$$C_{11} = -4\pi i\epsilon^2 V\left(\frac{F(1+\alpha\chi_s^0)+E}{U+J}\right) - 1 , \tag{24}$$

$$C_{21} = -4\pi i\epsilon^2 V \times\left(C + i\epsilon^2 + \frac{FA - i\epsilon^2(1+\alpha\chi_s^0)F - FB - EC - i\epsilon^2 E}{U+J}\right) \tag{25}$$

with

$$\frac{1}{U} = \sum_{m=-I}^{I}\frac{1}{G_m} , \tag{26}$$

$$V = [1 + \alpha\chi_s^0 E/(U+J)]^{-1} . \tag{27}$$

χ_s^0 is very small so that to first order in χ_s^0 the roots are

$$K_1^2 = K_{10}^2 + \chi_s^0 C_{21}/C_{10} , \tag{28}$$

$$K_2^2 = K_{20}^2 + \chi_s^0(C_{11} - C_{21}/C_{10}) , \tag{29}$$

where

$$K_{10}^2 = i\epsilon^2 , \tag{30}$$

$$K_{20}^2 = C_{10} - K_{10}^2 . \tag{31}$$

K_{10} just gives the usual propagation of the rf field into the skin depth. K_{20} describes the propagation of the spin magnetization into the sample.

In conventional ESR the experimentally measured quantity, when magnetic field modulation is used, is the derivative with respect to field of $\mathcal{P}$ (the power absorbed by the sample as the magnetic field is swept through resonance). We have

$$\mathcal{P} = (c/4\pi)\mathcal{H}_0 \operatorname{Im}(\mathcal{E}) , \tag{32}$$

where $\mathcal{H}_0$ is the rf magnetic field applied to the sample and $\mathcal{E}$ is evaluated at the surface. We will evaluate $\mathcal{P}$ only in the thick-sample limit. But, in order to also get the TESR signal, we will solve the boundary value problem for arbitrary thickness. We assume

$$\mathcal{H} = \mathcal{H}_1 + \mathcal{H}_2 = P\cosh k_1 z + Q\sinh k_1 z + R\cosh k_2 z + S\sinh k_2 z , \tag{33}$$

where $K_1^2 = \frac{1}{2}k_1^2\delta_e^2$ and $K_2^2 = \frac{1}{2}k_2^2\delta_e^2$. The constants P, Q, R, and S are determined from the boundary conditions

$$\mathcal{H}(-d/2) = \mathcal{H}_0 , \quad \mathcal{H}(d/2) = -b\mathcal{H}_0 , \tag{34}$$

$$\frac{\partial[\mathfrak{M}_s - \chi_s^0(\mathcal{H} + \alpha\chi_s^0\mathfrak{M}_d)]_{-d/2}}{\partial z = 0} , \quad \frac{\partial[\mathfrak{M}_s - \chi_s^0(\mathcal{H} + \alpha\chi_s^0\mathfrak{M}_d)]_{d/2}}{\partial z = 0} , \tag{35}$$

where we have taken $z = 0$ at the center of the sample. b is still to be determined and will yield the TESR signal. Equations (35) assume that a conduction electron striking the surface is reflected without any spin relaxation. We are using Walker's boundary condition rather than Kaplan's $\partial\mathfrak{M}_s/\partial z = 0$. In order to relate $\mathfrak{M}_s$ and $\mathfrak{M}_d$ to $\mathcal{H}$ we must simultaneously solve Eqs. (10) and (13)—a total of $2I+2$

equations. We find, since the equations are linear, that

$$\mathfrak{M}_{sn} = v_n \mathcal{H}_n , \quad \mathfrak{M}_{dn} = [v_n E/(U+J)]\mathcal{H}_n , \tag{36}$$

where $n = 1, 2$ and

$$v_n = \frac{1}{4\pi K_{10}^2}\left(\frac{(K_n^2 - K_{10}^2) + 4\pi\chi_s^0 F K_{10}^2/(U+J)}{1 - E/(U+J)}\right). \tag{37}$$

Note that v_1 is of order χ_s^0. To order χ_s^0, $\mathfrak{M}_d$ makes no contribution to the boundary condition. Then only the ratio $(v_1 - \chi_s^0)/(v_2 - \chi_s^0)$ appears in the calculation. When linearized in χ_s^0 this ratio becomes $\chi_s^0 T$, where we obtain

$$T = \frac{C_{21}}{C_{10}^2} + 4\pi K_{10}^2 \frac{(F+E)/(U+J) - 1}{C_{10}} . \tag{38}$$

By applying the four boundary conditions and linearizing in χ_s^0, we find

$$P = \frac{\mathcal{H}_0(1-b)}{2\cosh u}\left\{1 + \chi_s^0 \tanh u\left[-\frac{\sqrt{2}a\, C_{21}}{4K_{10}C_{10}} + \frac{K_{10}}{K_{20}} T \coth w\right]\right\},$$

$$Q = -\frac{\mathcal{H}_0(1+b)}{2\sinh u}\left\{1 + \chi_s^0 \coth u\left[-\frac{\sqrt{2}a\, C_{21}}{4K_{10}C_{10}} + \frac{K_{10}}{K_{20}} T \tanh w\right]\right\}, \tag{39}$$

$$R = -\frac{\mathcal{H}_0(1-b)K_{10}T\chi_s^0 \tanh u}{2K_{20}\sinh w} ,$$

$$S = \frac{\mathcal{H}_0(1+b)K_{10}T\chi_s^0 \coth u}{2K_{20}\cosh w} ,$$

where $u = aK_{10}/\sqrt{2}$, $w = aK_{20}/\sqrt{2}$, and $a = d/\delta_e$. In order to evaluate $\mathcal{E}$, use Eq. (33) in Eq. (11). When $b = -1$, the power absorbed reduces to Dyson's result. We will only consider the thick-sample limit, where u and w are very large and $b = 0$. By discarding the Joule heating term we find

$$\mathcal{P} = \eta\, \mathrm{Re}\left(\frac{(K_{20}+2K_{10})K_{10}}{K_{20}(K_{10}+K_{20})^2} C^* + \frac{K_{10}F^*}{U+J}\right) , \tag{40}$$

where

$$C^* = V(C+A) - \frac{V[E(C+A) + (E+F)B']}{U+J} + \frac{VE(E+F)B'}{(U+J)^2} , \tag{41}$$

$$F^* = E + F, \quad \eta = \sqrt{2}\, c^2 \mathcal{H}_0^2 \chi_s^0/8\pi\sigma\delta_e . \tag{42}$$

In TESR the measured quantity is the amplitude of the transmitted magnetic field. Magnetic modulation is not normally used, but the phase of the detector is adjusted to give a symmetric signal. From Eq. (34) we see that $\mathcal{H}_t = -b\mathcal{H}_0$. b is determined from the requirement that the transmitted field must be a traveling wave, that is, $|E_x(d/2)| = |H_y(d/2)|$ and $|E_y(d/2)| = |H_x(d/2)|$. In complex notation this requirement becomes $b\mathcal{H}_0 = i\mathcal{E}(d/2)$. We assume that u is large, that is, the sample is many skin depths thick, and we find

$$\mathcal{H}_t = \frac{K_{10}^4 \xi C^*}{(K_{20}^2 - K_{10}^2)^2 K_{20} \sinh 2w} , \tag{43}$$

where

$$w = dK_{20}/\sqrt{2}\delta_e$$

and

$$\xi = \chi_s^0 \mathcal{H}_0 c/\sqrt{2}\sigma\delta_e . \tag{44}$$

III. DISCUSSION AND NUMERICAL EVALUATION

The features of the line shape depend critically upon K_{20}. From Eqs. (24) and (31) we have

$$K_{20}^2 = [A - BE/(U+J)]V. \tag{45}$$

When there is no hyperfine interaction K_{20}^2 can be written in the form

$$K_{20}^2 = (\chi_s + \chi_d)(\chi_s^0)^{-1}[1 + iT_{eff}(\omega - \omega_0)]T_{sl}/T_{eff} - \xi T^*/T_{sl}[1 + T^*(\omega - \omega_d^*)] , \tag{46}$$

where

$$\omega_0 = \frac{\chi_s\omega_s + \chi_d\omega_d}{\chi_s + \chi_d} , \tag{47}$$

$$\frac{1}{T_{eff}} = \frac{\chi_s^0/T_{sl} + \chi_d^0/T_{dl}}{\chi_s + \chi_d} , \tag{48}$$

$$\omega_d^* = \omega_d(1 + \alpha\chi_s^0) , \tag{49}$$

$$\frac{1}{T^*} = \frac{1}{T_{ds}} + \frac{1}{T_{dl}} . \tag{50}$$

This expression is exact to order $\alpha\chi_s^0$. ξ is a complicated quantity which has only a slight dependence on $1/T_{ds}$. ξ is, in general, complex, but its imaginary part vanishes near ω_d^*. When hyperfine interaction is present, the expression for K_{20}^2 is much more complicated, but numerical calculation shows that a separation can be made similar to that of Eq. (46).

When only the first term in Eq. (46) is important we have the situation that has been called the bottleneck, where the resonant frequency and the linewidth have the very simple temperature dependence described by Schultz and co-workers[4] [Eqs. (47) and (48)]. The first term in Eq. (46) is independent of T_{ds} so that the cross relaxation enters into K_{20} only through the second term, where the width of the resonance at ω_d^* is determined by T_{ds}. Thus, the bottleneck holds when $1/\gamma T_{ds}$ is large enough to wipe out the second term. But note that it is not merely sufficient to have $1/\gamma T_{ds} \gg 1/\gamma T_{sl}$; it must also dominate over $1/\gamma T_{dl}$, $(\omega_d - \omega_s)/\gamma$, $\alpha\chi_s^0\omega/\gamma$,

and A_{hf}. Since the term bottleneck is traditionally associated with T_{s1} we will use the term strong coupling to denote the condition where the second term in Eq. (46) is negligible. This usage emphasizes that it is the size of the cross relaxation that determines the character of the resonance.

In order to understand the physical significance of our results we will combine computer calculation[16] and analytical evaluation of the line shape to discuss various special cases without regard to whether these cases correspond to actual physical situations We start with zero exchange, followed by strong coupling. We will then consider the two cases [see Eq. (7)] where strong coupling breaks down; (i) weak exchange and (ii) large d susceptibility (or low temperature). Finally, we consider several cases which correspond to possible experimental conditions.

A. Zero Exchange

When $\alpha = 0$, $B' = E = J = 0$, and $V = 1$. Then the ESR line shape [Eq. (40)] reduces to

$$\mathcal{P} = \eta \,\mathrm{Re}\left(K_{10}\,\frac{(K_{20}+2K_{10})(C+A)}{K_{20}(K_{10}+K_{20})^2} + K_{10}\,\frac{(E+F)}{U}\right). \tag{51}$$

The first term, which involves only the s-spin parameters, is the pure sample CESR line shape $\mathcal{P}_s$. It may be obtained from Dyson's results by taking $d \gg \delta$, δ_e, or from Kaplan's results by linearizing in χ_s^0. The drift current corrections to the Bloch equation and the boundary condition, which Kaplan and Dyson did not include, cancel each other out. Feher and Kip[9] have given the results of computer calculations of this line shape. The second term in Eq. (51), $\mathcal{P}_d$, is resonant at ω_d, or at the hyperfine frequencies, if there is a nuclear spin. This d resonance has a Lorentzian line shape since we have described $\vec{\mathbf{M}}_d$ by a Bloch equation. The factor K_{10} produces the mixture of absorption and dispersion signals expected from the phase change of the rf field as it propagates into the skin region. Note that for a given χ_r^0, when K_{10} becomes large, the intensity of the s line drops relative to the d line; $\mathcal{P}_s/\mathcal{P}_d = U(C+A)[K_{20}^2\,(E+F)]$ when $K_{10} \ll K_{20}$, but $\mathcal{P}_s/\mathcal{P}_d = 2U(C+A)/[K_{10}K_{20}(E+F)]$ when $K_{10} \gg K_{20}$. The reason for the drop in the CESR intensity is that when $K_{10} \ll K_{20}$ or $\delta_e \ll \delta$ the spins do not diffuse across the skin depth during their lifetime and thus remain in phase with H_1. But when $\delta_e \gg \delta$ the spins can diffuse across the skin depth and get out of phase with the rf fields, thereby reducing the power absorption. This effect shows that it is much more difficult to detect the CESR in a pure sample than the ESR of an impurity with the same susceptibility, and explains why TESR is more sensitive than CESR. The more pure one makes a sample, the more difficult it is to see its CESR.

The TESR line shape [Eq. (43)] reduces to

$$\mathcal{P} = \frac{\zeta(C+A)K_{10}^4}{(K_{20}^2 - K_{10}^2)^2 K_{20}}\,\frac{1}{\sinh 2w}\,, \tag{52}$$

which is the pure sample TESR signal. Again the drift current corrections cancel. Dunifer[17] has reported extensive calculations of this line shape. No d resonance occurs since the d spins are not mobile.

B. Strong Coupling

By strong coupling we mean that the field $1/\gamma T_{ds}$ is much larger than the other fields involved in the resonance—$1/\gamma T_{s1}$, $1/\gamma T_{d1}$, $(\omega_d - \omega_s)/\gamma$, $\alpha\chi_s^0\omega/\gamma$, and A_{hf}. When the coupling is strong, the resonant term $1/(U+J)$ is broadened by $1/\gamma T_{ds}$. Thus, in the region where K_{20} is resonant, C^* reduces to $C' = (1+\chi_r)[C + A + (2I+1)F]/(1 - \alpha\chi_s^0\chi_r)$, while $K_{10}(E+F)/(U+J)$ is negligible. This means that the ESR line shape is given by the first term in Eq. (51), except that $C+A$ must be replaced by C'. Likewise, the TESR line shape is obtained from Eq. (52) by replacing $C+A$ with C'. Thus, the line-shape expressions with impurities are unchanged from the pure sample line shapes as noted by Schultz *et al.* However, K_{20} is temperature dependent, which gives the resonance a temperature-dependent g shift and linewidth. This can easily be seen from Eq. (46), where for strong coupling the second term is negligible and K_{20}^2 is resonant at ω_0 with width $1/T_{eff}$. Note the slightly different dependence of ω_0 and $1/T_{eff}$ on the susceptibilities which implies different temperature dependences for the g shift and linewidth. Equation (46) can be reduced to the form of the pure sample expression $K_{20}^2 = 1 + i(\omega - \omega_s)T_{s1}$ by defining an effective spin depth $\delta_e' = [2DT_{eff}\chi_s^0/(\chi_s + \chi_d)]^{1/2}$.

In previous treatments, which neglected the drift current and relaxation toward the instananeous local field, $C+A$ and C' were both pure imaginary numbers so that the only way in which the magnetic impurities could affect the resonance was through K_{20}. But with these corrections we find C' has a real part;

$$C' = \frac{[(1+\alpha\chi_s^0)/T_{sd} - \chi_r^0/T_{d1} + i(\omega + \omega_d\chi_d/\chi_s^0)]T_{s1}(1+\chi_r)}{1 - \alpha\chi_s^0\chi_r}\,.$$

In order for strong coupling to hold, it is necessary that $1/T_{sd} \gg \alpha\chi_d^0\omega$. If in addition $1/T_{sd} \ll \omega$, then $\mathrm{Re}(C')$ can be neglected and a pure sample line shape is obtained. But if the coupling is so strong

that $1/T_{sd} \approx \omega$, then C' will mix the TESR absorption and dispersion signals. When the microwave phase is adjusted to make the minima equal, the over-all signal will not be symmetric and the peak of the resonance will not fall at ω_0. Thus, the temperature dependence of the peak g value will not be given by Eq. (47).

C. Weak Exchange

We now investigate the manner in which the transition is made from no coupling to the strong coupling limit. To do this we consider weak exchange and keep terms in the ESR line shape that are linear in $\alpha\chi_s^0$, neglecting $1/T_{ds}$. This approximation is always valid for small enough $\alpha\chi_s^0$ since by Eq. (7), $1/T_{ds} \propto (\alpha\chi_s^0)^2$. Then $B = \alpha\chi_s^0 \mathcal{C}$ and $E = \alpha\chi_s^0 F$. Equation (4) becomes approximately

$$\mathcal{P} = \mathcal{P}_s + \mathcal{P}_d - \frac{\alpha\chi_s^0 \mathcal{P}_s \mathcal{P}_d (2 + \epsilon^2/\omega T_{sl})}{K_{10}} \quad . \tag{53}$$

The exchange interaction admixes into each resonance a small amount of the other so that they become hybrid s-d lines. The degree of hybridization depends on the amount of overlap of the lines. Since the line shapes are basically Lorentzian, we only have to consider the overlap of the dispersion tails if the lines are separated by several linewidths. But the dispersion signal is antisymmetric so that whether the intensity of the line is increased or decreased by the admixture depends upon whether the overlapping line is at higher or lower field, as well as upon the sign of $\alpha\chi_s^0$. We find for negative (positive) exchange that the low- (high-) field line is enhanced. Figure 1 gives computer plots of the CESR line shape with weak positive and negative exchange for $\epsilon \ll 1$. The enhancement is clearly visible. The physical reason for the enhancement is that if the rf field H_1 is along the x axis in a rotating frame where H_1 is stationary and H_0 is near ω_s/γ, for example, then the s spins see an effective rf field $H_{1\,eff} = H_1 + \alpha M_{dx}$. Since M_{dx} yields the dispersion signal, it changes sign at ω_d/γ. Thus, for negative exchange and the s resonance at higher field than the d resonance, $H_{1\,eff} > H_1$ and the s resonance is enhanced. For the s resonance at lower field, $H_{1\,eff} < H_1$, and the s resonance is reduced.

Notice in Fig. 1 that there is also a g shift. We can evaluate this shift by taking $\mathcal{K} = 0$ in Eqs. (12) and (13) and setting the determinant of the coefficients equal to zero with no hyperfine interaction or diffusion. ω, then, is a complex number whose real part is the resonant frequency and whose imaginary part is the linewidth. We find

$$\begin{aligned} \omega_+ &= \omega_s(1 + \alpha\chi_d) + i(1/T_{sl} + 1/T_{sd}) \, , \\ \omega_- &= \omega_d(1 + \alpha\chi_s) + i(1/T_{dl} + 1/T_{ds}) \, . \end{aligned} \tag{54}$$

The shift is toward higher field (lower g) for negative exchange and lower field for positive exchange. It is clearly due to the exchange field adding to the external field. This is the shift that Owen, Brown, Knight, and Kittel[1] looked for when they studied Cu : Mn alloys. Note that exchange broadening is also predicted. However, our calculations show that as $\alpha\chi_s^0$ is increased, the enhancement effect becomes important long before exchange broadening enters.

From the foregoing we have this picture of the effect of adding increasing negative exchange: The low-field line, whether s or d, is enhanced and moves up in field, becoming the single strong coupling line with frequency ω_0. The high-field line loses intensity to the enhanced line, moves away from ω_0, and finally is totally obliterated by exchange broadening. For positive exchange the converse is true, with the high-field line being enhanced and moving down to ω_0.

When hyperfine interaction is present we can see from Eq. (53) that hybridization occurs separately with each hyperfine line. The effect is largest for the hyperfine lines nearest the s line. This is illustrated in Fig. 2, which shows the transition to strong coupling when $I = 1$.

The exchange terms appear in the TESR signal identically as in the ESR signal. Thus, s-d hybridization must occur even though the d resonance itself does not appear in the TESR. We can explain this by noting that, crudely speaking, the term $1/K_{20}\sinh 2w$ in Eq. (43) accounts for the propagation of the spin currents through the sample, while C^* satisfies the boundary conditions. When the d resonance occurs, the rf currents in the skin region are modified. The change in the spin currents required to continue satisfying the boundary conditions is then propagated through the sample. In Fig. 3, computer calculations of the

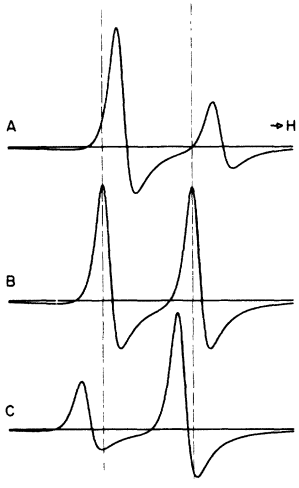

FIG. 1. Hybridization of ESR lines produced by weak exchange. $g_s = 2.033$, $g_d = 2.013$, $1/\gamma T_{sl} = 1/\gamma T_{dl} = 5$ G, $\delta_e/\delta = 0.01$, $\chi_r^0 = 1$, $\chi_r^0(1) = 1$, and A: $\alpha\chi_s^0 = -0.002$; B: $\alpha\chi_s^0 = 0$; C: $\alpha\chi_s^0 = +0.002$. The horizontal sweep range is 100 G. The signals are normalized to the same peak-to-peak height.

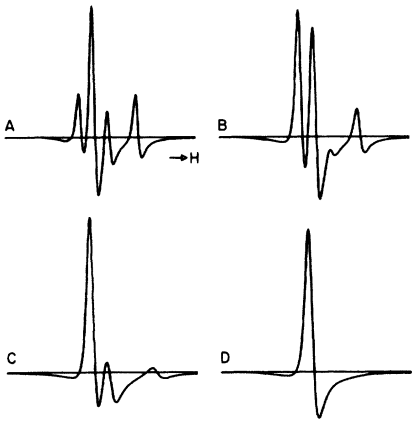

FIG. 2. ESR spectrum with hyperfine interaction as the exchange increases from weak to strong. $g_s = 2.033$, $g_d = 2.013$, $1/\gamma T_{sl} = 1/\gamma T_{dl} = 10$ G, $\delta_e/\delta = 0.01$, $\chi_r^0 = 1$, $\chi_r^0(1) = 1$, $A_{hf} = 60$ G, $I = 1$, and A: $\alpha\chi_s^0 = -0.0002$; B: $\alpha\chi_s^0 = -0.005$; C: $\alpha\chi_s^0 = -0.01$; D: $\alpha\chi_s^0 = -0.02$. The horizontal sweep range is 400 G. The signals are normalized the same peak-to-peak height.

TESR signal as the exchange is varied, showing that effects of the d resonance and even hyperfine splitting can be observed for intermediate strength exchange. Note that it is necessary to go to extremely small exchange to obtain the symmetric pure sample line shape.

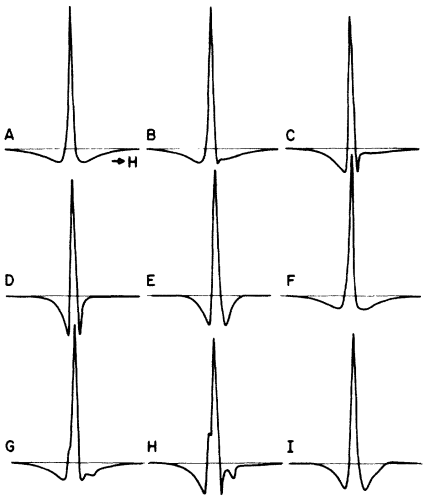

FIG. 3. TESR spectrum with and without hyperfine interaction as the exchange increases from weak to strong. $g_s = 2.033$, $g_d = 2.013$, $1/\gamma T_{sl} = 1/\gamma T_{dl} = 10$ G, $\delta_e/\delta = 100$, $d/\delta_e = 0.7$, $\chi_r^0 = 0.4$, $\chi_r^0(1) = 1$, and A: $\alpha\chi_s^0 = -0.00001$, $A_{hf} = 0$; B: $\alpha\chi_s^0 = -0.00007$, $A_{hf} = 0$; C: $\alpha\chi_s^0 = -0.0003$, $A_{hf} = 0$; D: $\alpha\chi_s^0 = -0.001$, $A_{hf} = 0$; E: $\alpha\chi_s^0 = -0.01$, $A_{hf} = 0$; F: $\alpha\chi_s^0 = -0.00007$, $A_{hf} = 60$ G, $I = 1$; G: $\alpha\chi_s^0 = -0.0003$, $A_{hf} = 60$ G, $I = 1$; H: $\alpha\chi_s^0 = -0.001$, $A_{hf} = 60$ G, $I = 1$; I: $\alpha\chi_s^0 = -0.01$, $A_{hf} = 60$ G, $I = 1$. The horizontal sweep range is 600 G. The signals are normalized to the same peak-to-peak height.

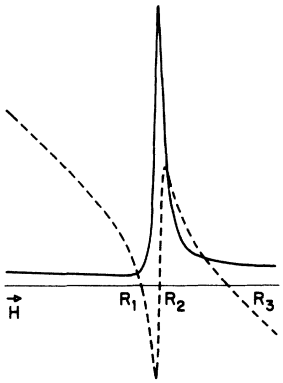

FIG. 4. Real and imaginary parts of K_{20}^2 vs magnetic field with $g_s = 2.033$, $g_d = 2.013$, $1/\gamma T_{sl} = 1/\gamma T_{dl} = 10$ G, $\chi_r^0 = 4$, $\chi_r^0(1) = 1$, $A_{hf} = 0$, and $\alpha\chi_s^0 = -0.02$. The horizontal sweep range is 1000 G. The vertical scale is arbitrary and not the same for both parts.

D. Large Exchange, Large χ_r^0

Equation (7) shows that strong coupling will break down even if $\alpha\chi_s^0$ is large, provided χ_r^0 becomes large enough, i.e., provided the temperature is low enough. The reason for this is simply that the s-spin system becomes too small to affect the d system; the d spin relaxation is dominated by direct (T_{dl}) relaxation to the lattice. Note, however, that even though $1/\gamma T_{ds}$ becomes very small when χ_r^0 is large, $1/\gamma T_{sd}$ can be large and the s system can be strongly affected by the d spins. As strong coupling breaks down, $1/T^*$ becomes small and the second term in Eq. (46) makes a contribution to K_{20}^2. Since ξ becomes real near ω_d, the effect of this term is to add a Lorentzian absorption component to $\mathrm{Re}(K_{20}^2)$ and a dispersion component to the imaginary part. These parts are plotted vs H in Fig. 4. We see that the imaginary part crosses zero three times, so that the resonance frequency is multivalued. These roots are not of equal importance in determining the nature of the TESR signal. Notice that the resonant character of R_2 is nullified by the resonant decrease in transmission produced by the peak in $\mathrm{Re}(K_{20}^2)$. As χ_r^0 increases, R_3 rapidly moves out to very high field. R_1 and R_2, on the other hand, move only slightly. Thus, the TESR signal is determined chiefly by R_1 with a high-field cutoff appearing because of the peak in $\mathrm{Re}(K_{20}^2)$, which damps out R_2. Note, however, that C^*, which is resonant at $\omega_d(1+\alpha\chi_s)$, also affects the TESR line. Figure 5 shows the variation of the TESR line shape as χ_r^0 is increased and strong coupling breaks down. R_3 is barely visible in Fig. 5(c). The narrowing of the line as χ_r^0 increases is due to the term $1/\sinh 2w$, which rapidly attenuates the signal when $\mathrm{Re}(K_{20}^2)$ becomes large. In Fig. 6 we compare the roots of $\mathrm{Im}(K_{20}^2)$ with the peak of the TESR signal and the strong coupling resonant frequency [Eq.

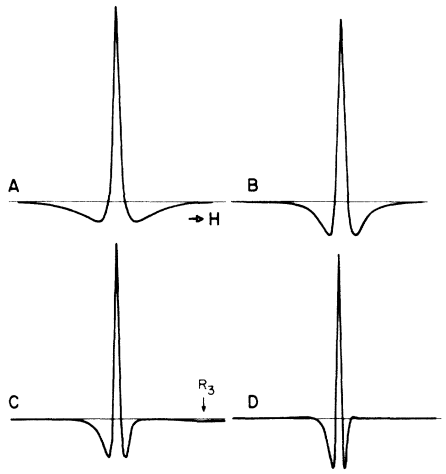

FIG. 5. Effect of the breakdown of strong coupling on the TESR spectrum without hyperfine interaction. $g_s = 2.033$, $g_d = 2.013$, $1/\gamma T_{sl} = 1/\gamma T_{dl} = 10$ G, $\delta_e/\delta = 100$, $d/\delta_e = 0.7$, $\chi_r^0(1) = 1$, $\alpha\chi_s^0 = -0.02$, $A_{hf} = 0$, and A: $\chi_r^0 = 0.1$; B: $\chi_r^0 = 1$; C: $\chi_r^0 = 4$; D: $\chi_r^0 = 10$. The horizontal sweep range is 600 G. The signals are normalized to the same peak-to-peak height.

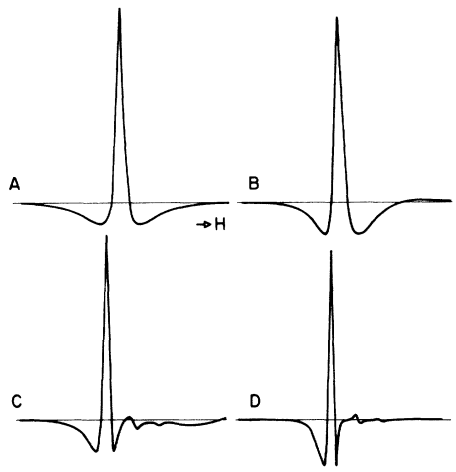

FIG. 7. TESR spectrum for the same parameters that are in Fig. 5 except $A_{hf} = 60$ G, $I = 1$.

(47)]. Notice that the strong coupling expression gives a reasonably good fit with the peak of the resonance throughout the region where the multiple roots of K_{20}^2 appear. A/B, the ratio of the low-field peak to the high-field peak decreases monotonically as χ_r^0 increases, although it does flatten in the region around $\chi_r^0 = 2$ where R_3 first appears. The linewidth decreases without flattening through this region. Figures 5 and 6 clearly show the inadequacy of the bottleneck concept. For the exchange used in these figures, $1/\gamma T_{sd} = 37.6$ and $T_{sl}/T_{sd} = 3.76$, so that the relaxation is moderately bottlenecked, yet the strong coupling line shape is not obtained except for very small χ_r^0.

When hyperfine interaction is added (Fig. 7), the TESR line shape is more complicated, but the same considerations apply as for $I = 0$. $\mathrm{Im}(K_{20}^2)$ has many roots arising from the hyperfine splitting (Fig. 8), but all except the lowest-field root are damped by resonant peaks in $\mathrm{Re}(K_{20}^2)$. Notice in Fig. 8 that the strong coupling formula breaks down for χ_r^0 an order of magnitude smaller than where K_{20}^2 first becomes multivalued. As in Figs. 5 and 6, $T_{sl}/T_{sd} = 3.76$ and the system is moderate-

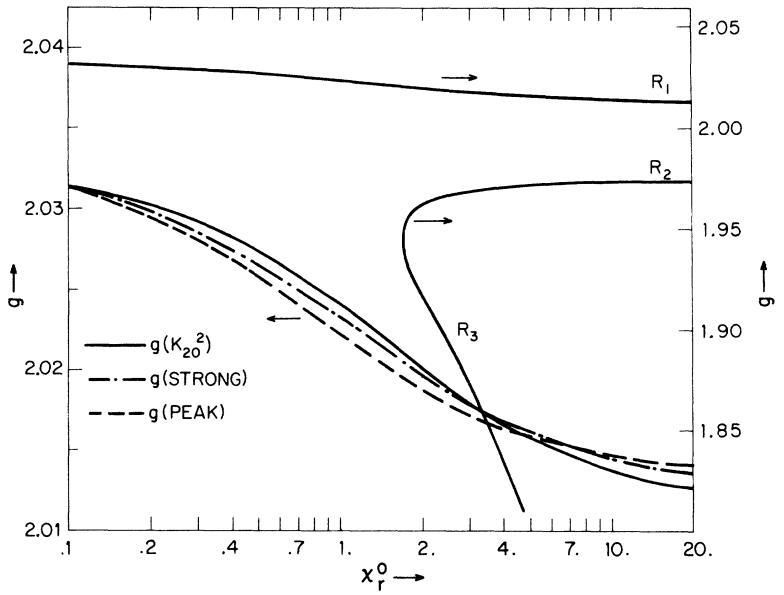

FIG. 6. g value of the peak of the TESR signal, the g value at which $\mathrm{Im}(K_{20}^2)$ vanishes, and the g value derived from the strong coupling expression [Eq. (47)] vs χ_r^0 for the parameters used in Fig. 5. R_1, R_2, and R_3, are the roots indicated in Fig. 4.

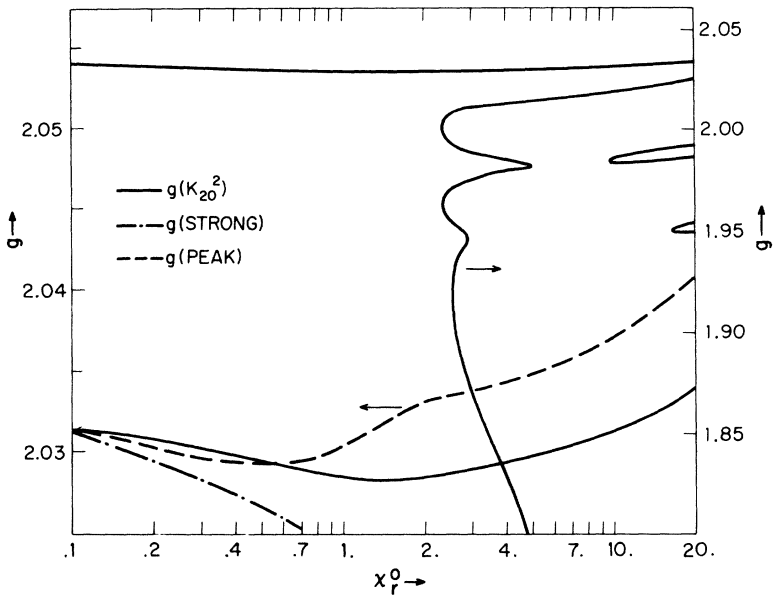

FIG. 8. Effect of hyperfine interaction on the g values in Fig. 6, $A_{hf} = 60$ G, $I = 1$.

ly bottlenecked. Figures 5–8 clearly show that when strong coupling does not hold it is totally inadequate to describe the line shape by evaluating the roots of K_{20}^2. Chui, Orbach, and Gehman[18] have reported $2I+1$ roots of $\mathrm{Im}(K_{20}^2)$ that appear

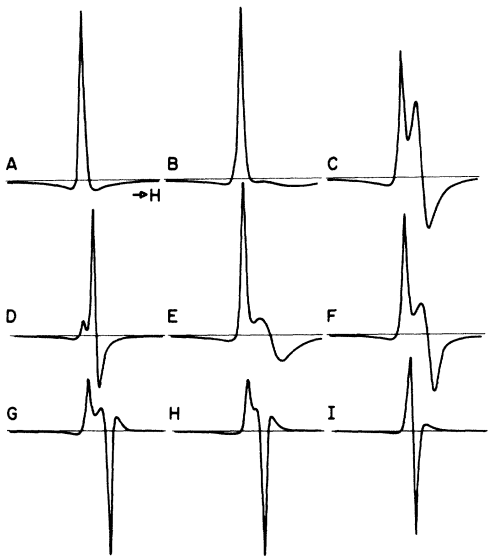

FIG. 9. Effect of the breakdown of strong coupling on the ESR spectrum. $g_s = 2.033$, $g_d = 2.013$, $1/\gamma T_{sl} = 1/\gamma T_{dl} = 10$ G, $\delta_e/\delta = 20$, $\chi_r^0(1) = 1$, $A_{hf} = 0$, and A: $\alpha\chi_s^0 = -0.02$, $\chi_r^0 = 0.1$; B: $\alpha\chi_s^0 = -0.02$, $\chi_r^0 = 0.4$; C: $\alpha\chi_s^0 = -0.005$, $\chi_r^0 = 0.4$; D: $\alpha\chi_s^0 = -0.0005$, $\chi_r^0 = 0.4$; E: $\alpha\chi_s^0 = -0.02$, $\chi_r^0 = 1$; F: $\alpha\chi_s^0 = -0.02$, $\chi_r^0 = 2$; G: $\alpha\chi_s^0 = -0.02$, $\chi_r^0 = 10$; H: $\alpha\chi_s^0 = -0.02$, $\chi_r^0 = 20$; I: $\alpha\chi_s^0 = -0.02$, $\chi_r^0 = 40$. The horizontal sweep range is 600 G. The signals are normalized to the same peak-to-peak height.

when $\omega_{hf} T_{ds} \gg 1$ are split by the hyperfine field and are spurious for zero hyperfine field. These reported roots correspond to the roots shown in Fig. 8. Note that although they are greatly modified when $A_{hf} = 0$, they are not spurious.

The breakdown of strong coupling has a somewhat different effect on the ESR line shape since large χ_r^0 makes the d resonance dominant. In Fig. 9 we show the line shape for several different values of χ_r^0. Figure 9(a) is the strong coupling line. As χ_r^0 is increased and strong coupling breaks down [Fig. 9(b)] a second hybrid resonance, broadened by cross relaxation, appears on the high-field side. If, at this point, the exchange is decreased [Figs. 9(c) and 9(d)], the second line grows in intensity and, in the limit of small exchange, can be identified as the d resonance. [Note in Fig. 9(d) that the s resonance is much smaller than the d resonance even though $\chi_r^0 = 4$. This is the attenuation effect for $\delta_e \gg \delta$ that we have discussed in the zero exchange section.] On the other hand, if $\alpha\chi_s^0$ is kept fixed at -0.02 and χ_r^0 is increased [Figs. 9(e)–9(g)], the second line grows in intensity but now cannot be identified as s- or d-like because, although strong coupling fails, the exchange is not weak. As χ_r^0 further increases [Figs. 9(h) and 9(i)], the two hybrid lines lose their s character and merge to form a single d line. This line is not simply due to the d term $K_{10}F^*/(U+J)$ in Eq. (40). The small A/B ratio and the peculiar line shapes in Figs. 9(g) and 9(h) are due to a drift current contribution in C^* which is not negligible even for large χ_r^0. This contribution rapidly disappears when ϵ is decreased. When hyperfine interaction is added (Fig. 10) the behavior

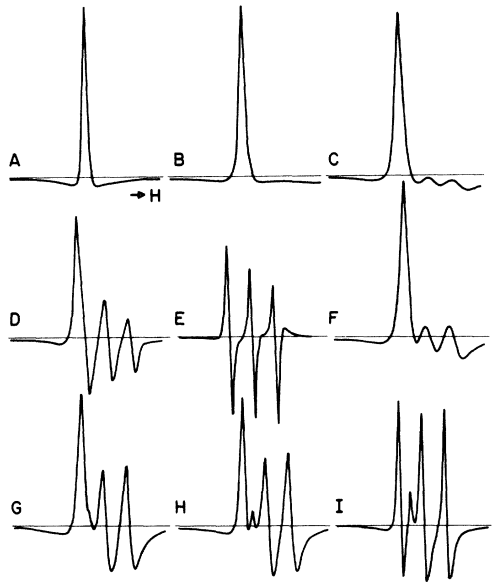

FIG. 10. ESR line shapes with the same parameters as in Fig. 8 except $A_{hf}=60$ G, $I=1$, and A: $\alpha\chi_s^0=-0.02$, $\chi_r^0=0.1$; B: $\alpha\chi_s^0=-0.02$, $\chi_r^0=0.4$; C: $\alpha\chi_s^0=-0.02$, $\chi_r^0=1$; D: $\alpha\chi_s^0=-0.02$, $\chi_r^0=4$; E: $\alpha\chi_s^0=-0.02$, $\chi_r^0=40$; F: $\alpha\chi_s^0=-0.01$, $\chi_r^0=0.4$; G: $\alpha\chi_s^0=-0.0075$, $\chi_r^0=0.4$; H: $\alpha\chi_s^0=-0.005$, $\chi_r^0=0.4$; I: $\alpha\chi_s^0=-0.001$, $\chi_r^0=0.4$.

of the line shape is similar, although complicated by the extra hyperfine lines.

E. Cu : Mn

The experimental TESR data[5] on Cr in Cu seems to be very well explained by the strong coupling limit without hyperfine interaction. However, Mn in Cu (and Ag) has been reported to be quite anomalous by Schultz, Shanabarger, and Platzman[4] (SSP): (i) The peak g value does not approach g_s as rapidly as the theory predicts at high T, (ii) the line shape is asymmetric with a long tail on the low-field side, (iii) in the most heavily doped samples $[\chi_r^0(1)\approx 65]$ the peak g value initially approaches g_d as T is lowered but then reverses and moves toward g_s, and (iv) samples with $\chi_r^0(1)\approx 37$ have a resonantlike peak in A/B near 7 °K which does not appear in samples whose impurity concentration differs by only a factor of 2. This A/B anomaly is not believed to be an intrinsic effect since it is not present in recent data.[19] In the following sections we discuss the application of our results to the Cu : Mn data.

1. *High-Temperature Plateau*

More accurate high-temperature measurements[19] than originally reported[4] make it possible to fit the high-temperature data to Hasegawa's theory without any plateau but at the expense of producing low-temperature deviations. However, our calculations show that the peak g value does not follow the temperature dependence of the true resonant g value [Eq. (47)] even at high temperature (≈ 20 °K), where strong coupling surely applies.[20] The reason is that C^* is a complex quantity dependent upon the magnetic field. The TESR signal is the component of H_t that is in phase with a reference rf field H_r. The phase of H_r differs from the phase of the field that excites the transmission by an angle θ, which can be arbitrarily varied. As θ is varied, the TESR signal changes from antisymmetric about the resonant field at $\theta=0$ to symmetric $\theta=\frac{1}{2}\pi$. When the data are taken, θ is varied to give a signal whose minima are equal. If C^* is imaginary, this setting corresponds to $\theta=\frac{1}{2}\pi$ and the signal is also symmetric. If C^* is a complex constant, a symmetric signal and equal minima are obtained for $\theta=\pi/2+\eta$, where $\tan\eta=C_1^*/C_2^*$ and $C^*=C_1^*+iC_2^*$. However, if C^* depends on H, and θ is adjusted to give equal minima, then near the resonant field there will be a mixture of the symmetric and antisymmetric signals which will shift the peak away from resonance. A very small amount of antisymmetric signal will produce a rather large g shift. In Fig. 11 we plot $\delta H/\Delta H$, the shift of the peak from the resonant field relative to the linewidth, vs $\alpha\chi_s^0$ for several impurity concentrations at 20 °K. For a linewidth of 100 Oe, $\delta H/\Delta H=0.015$ corresponds to $\delta g\simeq 0.001$. At 20 °K, $1/T_{ds}$ is large so that strong coupling holds except for small $\alpha\chi_s^0$ and large χ_r^0 (1), where we find a small effect due to hyperfine interaction. Note in

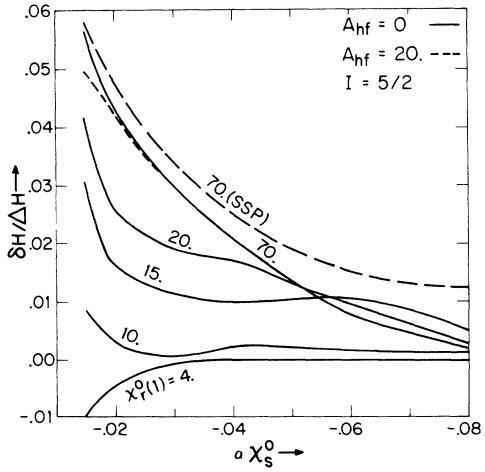

FIG. 11. Dependence of the shift of the peak of the TESR line from true resonance upon the exchange field and the impurity content. $T=20$ °K, $g_s=2.033$, $g_d=2.013$, $1/\gamma T_{dl}=15$ Oe, $\delta_e/\delta=50$, $d/\delta_e=0.7$. The dotted line shows that the hyperfine interaction has only a small effect at 20 °K. The dashed line is the apparent shift using Eq. (55) rather than Eq. (46) to determine the resonance field.

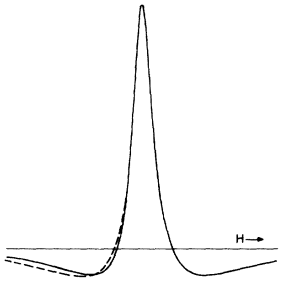

FIG. 12. Asymmetry in the TESR line shape at 20°K for the same parameters as in Fig. 11 and with $\alpha\chi_s^0 = -0.02$, $\chi_r^0(1) = 70$. The dotted line is the reflection about the peak of the high-field side.

Fig. 11 that if we had used SSP's equation for the resonant field,

$$\omega_{SSP} = (\chi_s^0 \omega_s + \chi_d^0 \omega_d)/(\chi_s^0 + \chi_d^0), \tag{55}$$

rather than Eq. (47), the apparent plateau would have been somewhat larger. For a given $\alpha\chi_s^0$, the size of the plateau increases with χ_r^0 (1) as reported by SSP. But for large χ_r^0 (1) this is not true, with the shift for χ_r^0 (1) = 40 (not shown) almost overlapping the shift for χ_r^0 (1) = 70. It is apparent that a large plateau in the g shift is indicative of weak exchange. However, we cannot use the size of the plateau to accurately evaluate $\alpha\chi_s^0$ since in addition to the strong dependence on $\alpha\chi_s^0$ and χ_r^0 (1) the shift also depends more weakly on T_{sl} and δ_e/δ. To obtain accurate values one must carefully fit all the data. Likewise, without careful fitting it is not possible to derive the true g value from the peak g value.

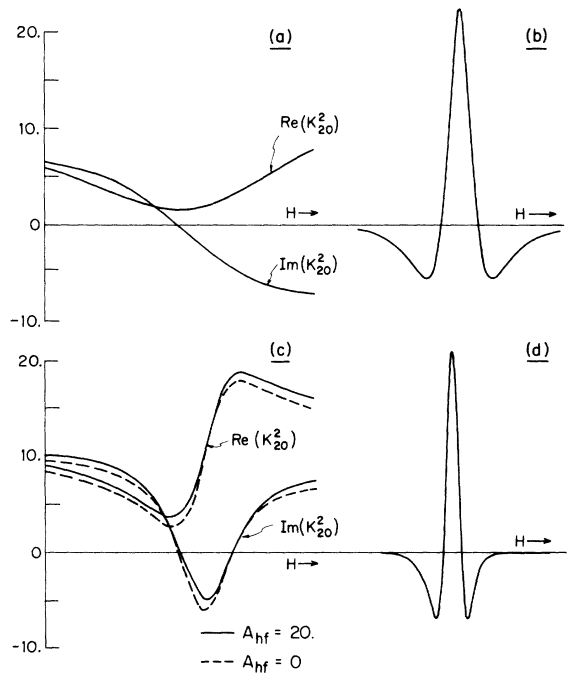

FIG. 13. (a) Real and imaginary parts of K_{20}^2 vs H at 10°K. $g_s = 2.033$, $g_d = 2.013$, $1/\gamma T_{sl} = 220$ Oe, $1/\gamma T_{dl} = 15$ Oe, $\alpha\chi_s^0 = -0.02$, $\delta_e/\delta = 50$, $d/\delta_e = 1.45$, $\chi_r^0(1) = 65$, $A_{hf} = 20$ Oe, $I = \frac{5}{2}$. H is varied over 800 Oe. (b) The line shape at 10°K. (c) Real and imaginary parts of K_{20}^2 at 2°K with $A_{hf} = 0$ and 20 Oe. (d) The line shape at 2°K with $A_{hf} = 20$ Oe.

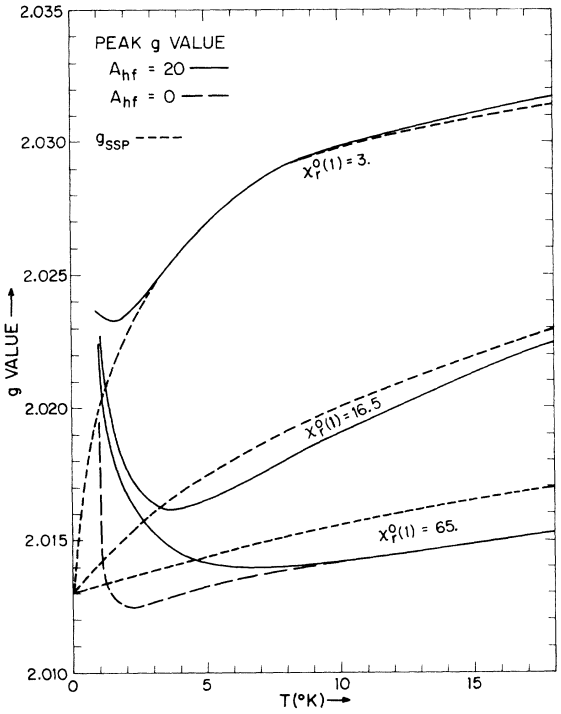

FIG. 14. Temperature dependence of the calculated peak g value for three different impurity concentrations. The dotted lines are derived from Eq. (55): $g_s = 2.033$, $g_d = 2.013$, $1/\gamma T_{dl} = 15$ Oe, $\alpha\chi_s^0 = -0.02$, $\delta_d/\delta = 50$, $A_{hf} = 20$ Oe, $I = \frac{5}{2}$. For $\chi_r^0(1) = 3$, $d/\delta_e = 0.7$ and $1/\gamma T_{sl} = 20$ Oe. For $\chi_r^0(1) = 16.5$, $d/\delta_e = 0.7$ and $1/\gamma T_{sl} = 65$ Oe. For $\chi_r^0(1) = 65$, $d/\delta_e = 1.45$ and $1/\gamma T_{sl} = 220$ Oe.

2. *Asymmetry*

We saw in Sec. III E 1 that the field dependence of C^* causes a mixture of the symmetric and antisymmetric TESR signals to produce a g shift. This mixture also produces an asymmetry in the line shape (Fig. 12). However, even with a large g shift, the asymmetry is rather modest. Note that the resonance has the longer tail on the high-field side.

There is another mechanism for producing asymmetry of a more drastic nature—the breakdown of strong coupling. This asymmetry is produced by a modification of K_{20} by the s-d interaction. We see from Eq. (46) that when the coupling is strong ($1/T_{ds}$ large), $\mathrm{Re}(K_{20}^2)$ is independent of H, while $\mathrm{Im}(K_{20}^2)$ varies linearly with H and vanishes at resonance. When $1/T_{ds}$ is smaller, the second term in Eq. (46) contributes a resonant character to both parts of K_{20}^2. In Fig. 13(a) we plot $\mathrm{Re}(K_{20}^2)$

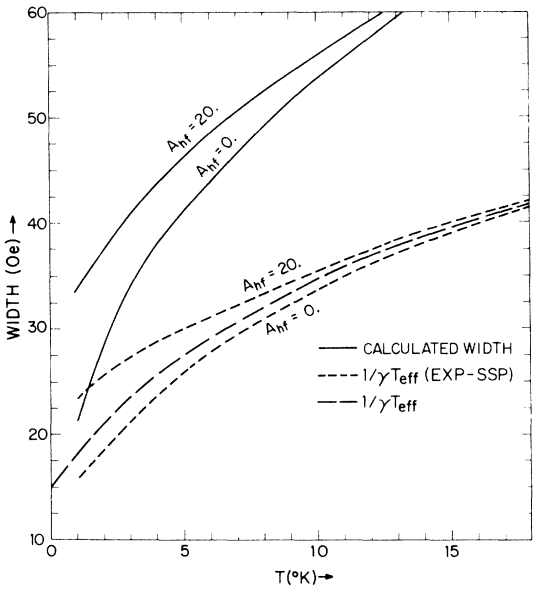

FIG. 15. Temperature dependence of the calculated linewidth (solid), $1/\gamma T_{\rm eff}$ (dashed) given by Eq. (48) and the apparent $1/\gamma T_{\rm eff}$ (dotted) that would be derived by correcting the linewidth by an amount determined from A/B using Schultz, Shanabarger, and Platzman's technique (Ref. 4). $g_s = 2.033$, $g_d = 2.013$, $1/\gamma T_{sl} = 65$ Oe, $1/\gamma T_{dl} = 15$ Oe, $\alpha\chi_s^0 = -0.02$, $\chi_r^0(1) = 16.5$, $\delta_e/\delta = 50$, $d/\delta_e = 0.7$, and $I = \frac{5}{2}$.

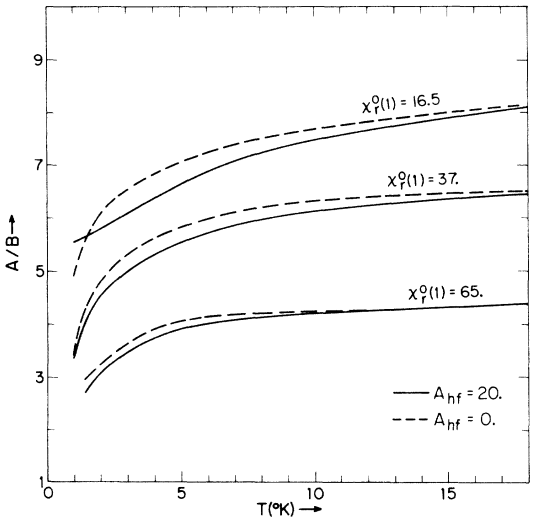

FIG. 16. Temperature dependence of the calculated asymmetry ratio for the same parameters as in Fig. 14. No anomaly is predicted at 7 °K for $\chi_r^0(1) = 37$. For $\chi_r^0(1) = 37$, $d/\delta_e = 0.9$ and $1/\gamma T_{sl} = 125$ Oe.

and $\mathrm{Im}(K_{20}^2)$ vs H at 10 °K for moderately strong exchange. We see that $\mathrm{Re}(K_{20}^2)$ is symmetric about resonance and the TESR line [Fig. 13(b)] is symmetric. Figures 13(a) and 13(b) are unchanged if hyperfine interaction is added. At 2 °K, $1/T_{ds}$ is reduced and strong coupling breaks down. $\mathrm{Im}(K_{20}^2)$ now has two resonant fields [Fig. 13(c)]. However, the sharp rise in $\mathrm{Re}(K_{20}^2)$, which corresponds to a sharp decrease in transmission, eliminates the high-field resonance. This decrease in transmission narrows the high-field side of the resonance

and produces an asymmetric line with a long low-field tail [Fig. 13(d)]. Note that the exchange coupling is strong enough so that the hyperfine interaction has a relatively minor effect on K_{20}^2. For the parameters used in Fig. 13, one would not expect resolved hyperfine structure on K_{20}^2 even with weaker coupling since $A_{\rm hf}$ is comparable to $1/\gamma T_{dl}$.

3. *Peak g Value*

The observed asymmetry and plateau in the peak g value both suggest that the exchange in Cu : Mn is not extremely large and strong coupling breaks down at low temperature. In Fig. 14 we plot the calculated peak g vs temperature for the three values of $\chi_r^0(1)$, for which SSP give data in Fig. 3 of their paper. The parameters chosen are roughly characteristic of Cu : Mn, with T_{sl} determined by the equation $1/\gamma T_{sl} = 10 + 3.3\chi_r^0(1)$ Oe and $\alpha\chi_s^0 = -0.02$ ($-J \approx 0.3$ eV). The hyperfine constant $A_{\rm hf} = 20$ Oe was determined from a very low-temperature measurement of the nuclear hyperfine field by Cameron *et al.*[21] Points above 20 °K are not included since phonon effects enter. The dotted lines in Fig. 14 give the temperature dependence

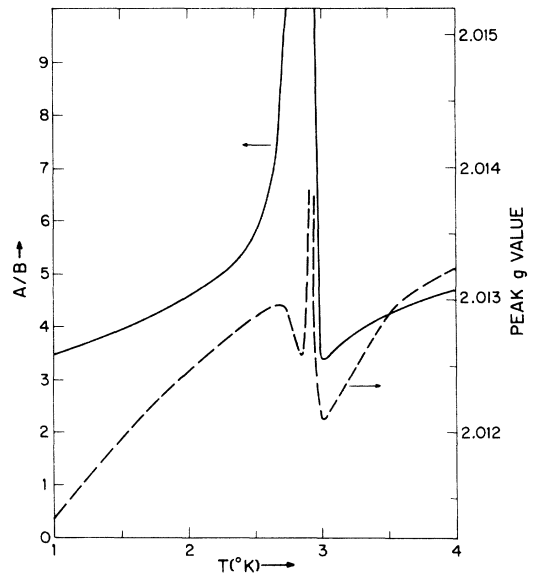

FIG. 17. A/B anomaly and peak g value for $\chi_r^0(1) = 37$. The anomalies appear when $\chi_r^0 = -1/\alpha\chi_s^0$. The same parameters are used as in Figs. 14 and 16 except $\alpha\chi_s^0 = -0.08$.

of SSP's strong coupling resonant frequency [Eq. (55)]. Comparison of the calculated peak g value with the experimental data shows qualitative agreement. The plateau for $\chi_r^0(1)=3$ is not correct. However, we have chosen $\delta_e/\delta=50$ for all three samples when, in fact, it should increase for pure samples. We also arbitrarily set $d/\delta_e=0.7$. Finally, at low-doping levels the anomalous skin effect, which we have neglected, may be important. Notice that at low temperature the g value turns up toward g_s. This was observed by SSP in concentrated samples and attributed to interactions between impurities. Interactions may be involved to some extent, but the up turn is also predicted by the LCW equations without impurity interactions. We see in Fig. 14 that, although the up turn is controlled by the hyperfine interaction, it occurs at much lower temperature even with $A_{hf}=0$. The origin of this effect is not due to any change in K_{20}^2 since we see in Fig. 13(c) that the positions of the roots of $\mathrm{Im}(K_{20}^2)$ change very little with A_{hf}. Rather, it is due to the emergence of the resonant part of C^*. When $A_{hf}=0$, C^* is resonant at $\omega_d'=\omega_d(1+\alpha\chi_s)$, while K_{20} is resonant at $\omega_d^*=\omega_d(1+\alpha\chi_s^0)$. For small χ_r^0 the difference between χ_s and χ_s^0 is negligible, but at low temperature with negative exchange, χ_s becomes considerably smaller than χ_s^0. This moves the C^* resonance to larger g, producing the shift in the peak. This shift cannot continue indefinitely since transmission occurs only in the vicinity of ω_d^*. When A_{hf} is nonzero the hyperfine splitting of C^* makes the up turn appear at higher temperature even though the splitting is symmetric about ω_d' because the asymmetry in $\mathrm{Re}(K_{20}^2)$ attenuates the high-field hyperfine contributions to C^*.

4. *Linewidth*

As predicted by LCW[6] the line is broadened by the hyperfine interactions. In Fig. 15 we compare the calculated linewidth vs temperature for $A_{hf}=0$ and 20 Oe. In order to obtain values for $\chi_r^0(1)$ and T_{dl}, SSP fit the linewidth to the theoretical width $1/T_{eff}$. To do this one must know $\Delta H\gamma T_{eff}$. SSP's theory asserts that this quantity is uniquely related to A/B. This is not the case for our solution. Applying SSP's technique to the widths in Fig. 15 makes $1/\gamma T_{dl}$ (the $T=0$ intercept) too large and $\chi_r^0(1)$ too small. Note that this technique will not give correct values even if $A_{hf}=0$. One is forced to fit all the data at once.

5. *A/B*

Our calculations (Fig. 16) show a monotonic increase in A/B with temperature and only a weak dependence on A_{hf}. Although the A/B anomaly appears to be an experimental artifact, we have found two mechanisms which can theoretically produce peaks in A/B at low temperature. The first mechanism is simply the breakdown in strong coupling due to large large χ_r^0. For slightly smaller exchange ($\alpha\chi_s^0\approx-0.015$) breakdown produces an A/B anomaly in the temperature range 1–2 °K that has the character of a shoulder or small bump rather than a resonant peak of the type observed by SSP. The second mechanism is the vanishing of χ_s [Eq. (8)] when $\chi_r^0=-1/\alpha\chi_s^0$. This is the condition where, for negative exchange, the exchange field exactly cancels the static magnetic field. In the temperature region where χ_r^0 is near this critical value, A/B has a sharp peak going to infinity. For $\alpha\chi_s^0=-0.02$ and $\chi_r^0(1)=37$, the anomaly appears below 1 °K. Figure 17 shows that even for $\alpha\chi_s^0=-0.08$ the peak occurs below 3 °K. There is very little dependence on A_{hf}. Note that the width of the peak is only $\simeq 0.5$ °K and an anomaly appears in the peak g value as well as in the linewidth. Caution must be used with these very low-temperature predictions since the LCW equations assume $\gamma hH/kT\ll 1$.

F. $\delta_e/\delta\ll 1$

This limit applies to degenerate semiconductors where the skin depth is large due to the small carrier concentration but the spin depth is small due to the rapid spin-flip scattering by the donors. There can be no TESR signal for this case. The ESR signal becomes very simple; we obtain

$$\mathcal{P}=\eta\,\mathrm{Re}\,K_{10}[C^*/K_{20}^2+F/(U+J)]\,. \tag{56}$$

When the coupling is large, the second term is exchange broadened and C^* is imaginary, provided the exchange is not too large as discussed in Sec.

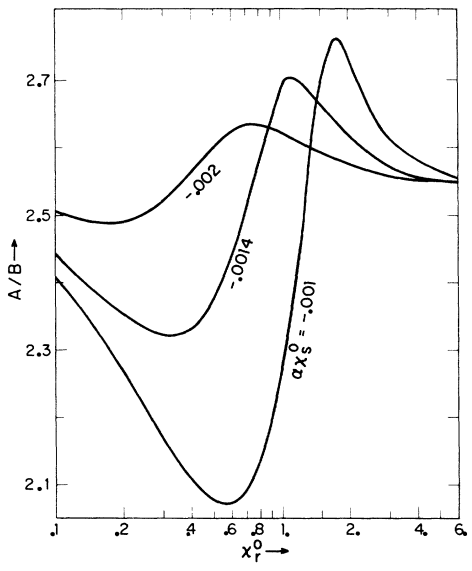

FIG. 18. A/B vs χ_r^0 for the ESR line shape with $g_s=1.999$, $g_d=2.000$, $1/\gamma T_{sl}=3$ G, $1/\gamma T_{dl}=6$ G, $\delta_e/\delta=0.01$, and $\chi_r^0(1)=0.5$.

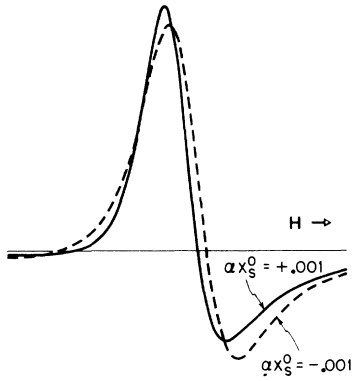

FIG. 19. The effect of the sign of the exchange on the ESR line shape for the same parameters as in Fig. 18 and $\chi_r^0 = 0.4$. For $\alpha\chi_s^0 = -0.001$, $A/B = 2.10$, while for $\alpha\chi_s^0 = +0.001$, $A/B = 2.72$.

III B. We then have a single Lorentzian line. This line is an admixture of equal parts of the real and imaginary components since $K_{10} = \epsilon(1+i)^{-1/2}$. Numerical evaluation shows that this admixture produces an A/B ratio of 2.55. At the other extreme, when the coupling is small, both terms contribute Lorentzian lines. Since C^* and F are imaginary, A/B is again 2.55.

This line-shape study was originally motivated by our observation[22,23] that in degenerate Si : P doped with Fe, a single resonance occurs with a temperature-dependent g shift, linewidth, and A/B ratio. A/B becomes as small as 2.0 at low temperature. We can see that this decrease in A/B can occur if C^* has a nonzero real part, which will occur with intermediate strength exchange. However, when we impose the requirement that only a single line should appear with no resolved structure, we find that A/B can deviate from 2.55 for only a very small range of parameters. Figure 18 shows A/B vs χ_r^0 for parameters typical for (Si : P) : Fe. Since g_s and g_d are so close and $\alpha\chi_s^0$ is so weak, one might suspect that this deviation of A/B from 2.55 is merely due to the addition of two independent lines. However, in Fig. 19 we can see that the sign of the exchange is critical. When $\alpha\chi_s^0 = 0$ for the same parameters, $A/B = 2.47$. The results of attempts to fit this theory to the data are reported separately.[23]

IV. CONCLUSION

We have evaluated the ESR and TESR line shapes in a metal containing magnetic impurities for the general case of arbitrary exchange, hyperfine interaction, and nuclear spin, but we have neglected the possibility of anomalous skin effect. We have shown that the size of T_{sl} relative to T_{sd} is not an adequate test to determine the nature of the resonance signal. In our discussion we have discarded this concept of the bottleneck and have emphasized that the character of the line shape is determined by the strength of the T_{ds} coupling relative to the spin-lattice relaxation times, the line separation, the exchange fields, and the hyperfine splitting. We find that apart from the limiting cases of strong or weak coupling, the spectra may be complex with the number of lines, g shift, width, and asymmetry depending upon the exact values of the parameters. Despite this complexity, we have been able to develop a physical picture of the factors determining these spectra. We have found that there are many cases where the coupling is not strong, yet a single line is observed which is hard to distinguish from the strong coupling line and that is is not sufficient to describe the resonance in terms of the roots of K_{20}^2.

We have compared the theory with the published Cu : Mn transmission-resonance data and have shown that the anomalies can be explained as a combination of effects due to hyperfine interaction and a breakdown of strong coupling at low temperature. A careful fitting of a wide range of experimental data should provide accurate values for the exchange and the hyperfine constant.

ACKNOWLEDGMENTS

We are grateful to the Rutgers Bubble Group for the extensive use of their PDP-6 computer. We would also like to thank Professor D. C. Langreth for many useful discussions.

*Work supported in part by the National Science Foundation.

†Present address: California State College at Los Angeles, Los Angeles, Calif.

[1]J. Owen, M. Browne, W. D. Knight, and C. Kittel, Phys. Rev. 102, 1501 (1956).

[2]H. Hasegawa, Progr. Theoret. Phys. (Kyoto) 21, 483 (1959).

[3]A. C. Gossard, A. J. Heeger, and J. H. Wernick, J. Appl. Phys. 38, 1251 (1967); A. C. Gossard, T. Y. Kometani, and J. H. Wernick, *ibid.* 39, 849 (1968).

[4]S. Schultz, M. R. Shanabarger, and P. M. Platzman, Phys. Rev. Letters 19, 749 (1967).

[5]P. Monod and S. Schultz, Phys. Rev. 173, 645 (1968).

[6]D. C. Langreth, D. L. Cowan, and J. W. Wilkins, Solid State Commun. 6, 131 (1968); and unpublished.

[7]J. I. Kaplan, Phys. Rev. 115, 575 (1959).

[8]H. C. Torrey, Phys. Rev. 104, 563 (1956).

[9]G. Feher and A. F. Kip, Phys. Rev. 98, 337 (1955).

[10]J. H. Pifer and R. Magno, Phys. Rev. B 3, 663 (1971).

[11]G. D. Gaspari, Phys. Rev. 151, 215 (1966).

[12]F. J. Dyson, Phys. Rev. 98, 349 (1959).

[13]M. B. Walker, Phys. Rev. B 3, 30 (1971).

[14]M. Lampe and P. M. Platzman, Phys. Rev. 150, 340 (1966).

[15]G. E. H. Reuter and E. H. Sondheimer, Proc. Roy. Soc. (London) A195, 336 (1948).
[16]The calculations were done on the Rutgers Bubble Chamber Group's PDP-6 computer which is supported in part by the National Science Foundation.
[17]G. L. Dunifer, thesis (University of California, 1968) (unpublished).
[18]R. Chui, R. Orbach, and B. L. Gehman, Phys. Rev. B 2, 2298 (1970).
[19]S. Schultz (private communication).
[20]Above 20°K phonon relaxation rapidly increases $1/\gamma T_{sl}$ and strong coupling again breaks down.
[21]J. A. Cameron, I. A. Campbell, J. P. Compton, R. A. G. Lines, and G. V. H. Wilson, Phys. Letters 20, 569 (1966).
[22]R. T. Longo and J. H. Pifer, Bull. Am. Phys. Soc. 15, 95 (1970).
[23]R. T. Longo and J. H. Pifer (unpublished).

PHYSICAL REVIEW B VOLUME 4, NUMBER 11 1 DECEMBER 1971

Transmission of U^{235} Fission Fragments in Solid Media

V. Aiello,* G. Maracci, and F. Rustichelli†
Physics Division, Joint Research Center, Euratom, Ispra, Italy
(Received 6 April 1971)

Transmission measurements of the fission fragments arising in U^{235} thermal-neutron-induced fission were performed in Mg, Al, Fe, and Ag by using a back-to-back fission chamber. From the transmission curves, it is possible to derive the relative atomic stopping powers of the different targets and the ranges of the fission fragments in the elements investigated. The experimental results are compared with the theoretical calculations of Lindhard, Scharff, and Schiøtt concerning the loss of energy of heavy ions in matter.

INTRODUCTION

Much experimental information is available concerning the energy loss of charged particles in matter. The parameters which are varied from experiment to experiment are the mass numbers, the atomic numbers, the electrical charges and the energies of the incident particles, and the mass numbers and the atomic numbers of the stopping materials.

Lindhard, Scharff, and Schiøtt (LSS)[1] have developed a general theory for the energy loss of heavy ions in matter, using a Thomas-Fermi statistical model for interacting atoms to predict both electronic and nuclear stopping powers. Their theory, which does not contain adjustable parameters, resulted in agreement with a wide class of different experiments[1] previously performed. Most of the subsequent experimental results[2–31] were compared with the LSS theory, which generally appears to be able to explain the fundamental mechanism of the loss of energy of charged particles.

However, there are several cases in which the theory shows some discrepancies from the experimental values. For instance, an oscillatory dependence of the electronic stopping cross section on the atomic number Z_1 of the projectile was observed[9] for Al and C. Also, an oscillatory dependence on the atomic number Z_2 of the stopping element was observed[29] by using α particles as projectiles. This behavior is not foreseen by the unmodified LSS theory, which gives a monotonic dependence of the stopping cross section on both Z_1 and Z_2.

The present experiment consists of transmission measurements on the fission fragments arising in U^{235} thermal-neutron-induced fission. The stopping elements Mg, Al, Fe, and Ag were used. From the transmission curves it is possible to derive the relative atomic stopping powers of the different target elements and the corresponding ranges. The aim of the experiment was to add new data to those existing in the field of energy loss of U^{235} fission fragments and to test the LSS theory for the dependence of the stopping power for fission fragments on the atomic number Z_2 of the stopping element.

EXPERIMENTAL METHOD

The method utilized is practically the same as that of Segrè and Wiegand.[32] The measurements were carried out by irradiating a back-to-back fission chamber (Fig. 1) in the thermal column of the RB-2 reactor of Montecuccolino (Bologna). The double fission chamber[33] is a gas flow counter utilizing argon containing 2% nitrogen. The electrode spacing was 10 mm and the gas pressure was adjusted slightly above ambient pressure. The operating voltage was 500 V positive applied to each anode. The fission-fragment source was a thin deposit of natural uranium, with a thickness of 0.2 mg/cm^2 and a diameter of 12 mm, obtained by vacuum evaporation on a Pt disc of 0.1-mm thickness and 20-mm diameter. The amount of fissionable material was determined with an ac-